1 **Multiple pathways for the formation of secondary organic aerosol in North China Plain**

2 **in summer**

3 Yifang Gu[1,4], Ru-Jin Huang[1,2,3,4], Jing Duan[1], Wei Xu[1], Chunshui Lin[1], Haobin Zhong[1,4], Ying

4 Wang[1], Haiyan Ni[1], Quan Liu[5], Ruiguang Xu[6,7], Litao Wang[6,7], Yong Jie Li[8]

5 [1]SKLLQG, Center for Excellence in Quaternary Science and Global Change, Institute of Earth

6 Environment, Chinese Academy of Sciences, Xi'an 710061, China

7 [2]Open Studio for Oceanic-Continental Climate and Environment Changes, Pilot National

8 Laboratory for Marine Science and Technology (Qingdao), Qingdao 266000, China

9 [3]Institute of Global Environmental Change, Xi'an Jiaotong University, Xi'an 710049, China

10 [4]University of Chinese Academy of Sciences, Beijing 100049, China

11 [5]State Key Laboratory of Severe Weather & Key Laboratory of Atmospheric Chemistry of C

12 MA, Chinese Academy of Meteorological Sciences, Beijing 100081, China

13 [6]Department of Environmental Engineering, School of Energy and Environmental Engineering,

14 Hebei University of Engineering, Handan 056038, China

15 [7]Hebei Key Laboratory of Air Pollution Cause and Impact, Handan 056038, China

16 [8]Department of Civil and Environmental Engineering, and Centre for Regional Oceans, Faculty

17 of Science and Technology, University of Macau, Taipa, Macau 999078, China

18 *Correspondence to*: Ru-Jin Huang (rujin.huang@ieecas.cn)

Abstract

Secondary organic aerosol (SOA) has been identified as a major contributor to fine particulate matter ($PM_{2.5}$) in North China Plain (NCP). However, the chemical mechanisms involved are still unclear due to incomplete understanding of its multiple formation processes. Here we report field observations in summer in Handan of NCP, based on high-resolution online measurements. Our results reveal the formation of SOA via photochemistry and two types of aqueous-phase chemistry, the latter of which include nocturnal and daytime processing. The photochemical pathway is the most important under high O_x ($=O_3 + NO_2$) conditions (65.1 ± 20.4 ppb). The efficient SOA formation from photochemistry (O_x-initiated-SOA) dominated the daytime (65% to OA) with an average growth rate of $0.8\,\mu g\,m^{-3}\,h^{-1}$. During the high relative humidity (RH: 83.7 ± 12.5 %) period, strong nocturnal aqueous-phase SOA formation (aq-SOA) played a significant role in SOA production (45% to OA) with a nighttime growth rate of 0.6 $\mu g\,m^{-3}\,h^{-1}$. Meanwhile, an equally fast growth rate of 0.6 $\mu g\,m^{-3}\,h^{-1}$ of O_x-initiated-SOA from daytime aqueous-phase photochemistry was also observed, which contributed 39% to OA, showing that photochemistry in the aqueous phase is also a non-negligible pathway in summer. The primary-related-SOA (SOA attributed to primary particulate organics) and aq-SOA are related to residential coal combustion activities, supported by distinct fragments from polycyclic aromatic hydrocarbons (PAHs). Moreover, the conversion and rapidly oxidation of primary-related-SOA to aq-SOA could be possible in the aqueous phase under high-RH conditions. This work sheds light on the multiple formation pathways of SOA in ambient air of complex pollution, and improves our understanding of ambient SOA formation and aging in summer with high oxidation capacity.

KEYWORDS: secondary organic aerosol, aqueous-phase chemistry, photochemistry, multiple-phase chemistry, complex air pollution

1. Introduction

Rapid economic growth and urbanization processes have led to severe particulate air pollution in China, affecting air quality, climates and human health (Huang et al., 2014; Cohen et al., 2017; An et al., 2019). Organic aerosol (OA) is a major component of aerosol particles, consisting of 20-90% of fine particle mass (Jimenez et al., 2009; Zhang et al., 2011). OA is either emitted directly from primary sources (referred to as primary OA, POA) such as traffic, cooking, coal combustion, and biomass burning, or produced through gas-to-particle conversion (referred to as secondary OA, SOA) in the atmosphere. In recent years, with the implementation of control measures, the POA fraction is decreasing and SOA fraction is increasing in North China Plain (NCP), indicating that SOA is becoming more critical for urban air quality (Huang et al., 2019; Xu et al., 2019; Gu et al., 2020). However, our understanding of the formation mechanisms and evolution processes of SOA is still limited.

Generally, SOA can be formed through gas-phase photochemical oxidation of volatile organic compounds (VOCs) followed by nucleation or condensation of oxidation products onto the preexisting particles (Donahue et al., 2006). Herndon et al., (2008) showed that oxygenated organic aerosol (OOA), a surrogate of SOA, was well correlated with odd oxygen ($O_x = O_3 + $ nitrogen dioxide (NO_2)) during photochemical processing. SOA can also be formed in the aqueous phase on wet aerosols, clouds and fogs through further chemical processes of water-soluble organic compounds or organic products of gas-phase photochemistry (Ervens et al., 2011, 2014). A growing number of laboratory studies and field measurements have indicated that aqueous-phase processes contribute efficiently to the formation of SOA (Gilardoni et al., 2016; Bikkina et al., 2017). However, how photochemistry and aqueous-phase chemistry coordinate to affect the formation of SOA is still unclear, despite numerous measurements to explore this question using aerosol chemical speciation monitor (ACSM) or aerosol mass spectrometer (AMS) (Hu et al., 2016b; Hu et al., 2017; Sun et al., 2016; Li et al., 2017; Sun et al., 2018b; Huang et al., 2019; Gu et al. 2020; Kuang et al., 2020). Field measurements in Beijing suggested that gas-phase photochemical oxidation can play a dominant role in SOA formation (Sun et al., 2016; Hu et al., 2016a). Xu et al., (2017) showed that less oxidized-OOA (LO-OOA) was mainly formed through photochemical oxidation, while the more oxidized-OOA (MO-OOA) formation was dominantly formed by aqueous-phase chemistry in Beijing for different seasons. Kuang et al. (2020) investigated the effects of gas-phase and aqueous-phase photochemical processes on the formation of SOA and found that photochemical aqueous-phase SOA formation dominantly contributed to daytime OOA formation in winter Gucheng, located between Beijing (∼100 km) and Baoding (∼40 km) on the NCP. We found that photochemical processing attributed mostly to MO-OOA in summertime Beijing (Gu et al., 2020). Although these studies provided important insights into SOA formation processes, our understanding on the photochemical and aqueous-phase formation pathways for SOA and their

impacts on oxidation degree are far from complete. This lack of understanding is especially so under the conditions that atmospheric oxidative capacity and pollution characteristics have been largely changing in China due to large reduction in direct emissions of air pollutants.

In this study, we investigated the photochemical versus aqueous-phase processing for SOA composition and oxidation degree of OA in summertime Handan, which is a typical industrialized city in the NCP region. The city is located at the intersectional area of Hebei, Shanxi, Henan, and Shandong–four heavily urbanized and industrialized provinces (Fig. S1), and it is therefore an ideal site to investigate the SOA formation pathways in the NCP region. The multiple formation pathways, evolution of SOA composition, and oxidation degree under different meteorological conditions were discussed, which sheds light on the aqueous-phase chemistry and photochemical processing in SOA formation in the NCP region of China.

2. Experimental methods

2.1 Sampling site

Measurements were conducted from 10th August 2019 to 17th September 2019 on the campus of Hebei University of Engineering (36.57 °N, 114.50 °E), located at the southeast edge of urban Handan (Fig. S1). The site is surrounded by a school and residential areas, ~300 m north to South Ring Road and ~400 m northeast to the Handan Highway (S313). The sampling site is on the rooftop of a four-floor building, approximately 12 m above the ground.

2.2 Instrumentation

Real-time non-refractory $PM_{2.5}$ composition was measured by a soot particle long time-of-flight aerosol mass spectrometer (SP-LToF-AMS, Aerodyne Research Inc.) with a time resolution of 1 min. The detailed instrument description and operation of AMS were reported in Onasch et al., (2012). Compared to the conventional AMS, the LToF mass analyzer can provide much better mass resolution of ∼8000. During the campaign, the instrument was operated in the "laser off" mode and only the standard tungsten vaporizer was applied. Therefore, only non-refractory $PM_{2.5}$ components (NR-$PM_{2.5}$) were measured, including organics (Org), nitrate (NO3), sulfate (SO4), ammonium (NH4), and chloride (Chl). Ambient air was sampled and dried by a Nafion dryer (MD-700-24S, Perma Pure, Inc.) at a flow rate of 5 L min^{-1}, and then sub-sampled into the SP-LToF-AMS at a flow rate of ~ 0.1 L min^{-1}. An aerodynamic $PM_{2.5}$ lens was used to focus the particle into a beam, which was then impacted on the heated tungsten surface (~ 600 °C) and flash-vaporized. Electron ionization with 70 eV was used to ionize the vaporized gases. The ionization efficiency (IE) and the relative ionization efficiency (RIE) calibrations (Jimenez et al., 2003) were conducted by using 350 nm ammonium nitrate (NH_4NO_3) and ammonium sulfate ((NH_4)$_2SO_4$) particles.

118   Gaseous pollutants including SO_2 (9850 SO_2 analyzer, Ecotech), NO_2 (Model 42i NO-NO$_2$-

119   NO$_x$ analyzer, Thermo Scientific), CO (Model 48i carbon monoxide analyzer, Thermo

120   Scientific), O_3 (Model 49i ozone analyzer, Thermo Scientific), and meteorological parameters

121   including RH and temperature were also measured during the observation period. Furthermore,

122   an aethalometer (Model AE-33, Magee Scientific) was deployed to measure the mass

123   concentration of black carbon (BC) at a time resolution of 1 min.

124   **2.3 Data Analysis**

125   The data analysis software (SQUIRREL, version 1.63I and PIKA, 1.23I) within Igor Pro 6.37

126   (WaveMetrics) was used to analyze the AMS data. The experimental RIE values of 4 (NH4)

127   and 1.2 (SO4) and the standard RIE values of 1.4 (Org), 1.1 (NO3) and 1.3 (Chl) were used.

128   The composition-dependent collection efficiency (CDCE, Middlebrook et al., 2012) was used

129   to compensate for the incomplete detection caused by particle bounce on the vaporizer. An

130   improved Ambient (I-A) method was adopted for the elemental ratio analysis of high-resolution

131   (HR) OA mass spectra, such as oxygen-to-carbon (O:C), and hydrogen-to-carbon (H:C) ratios

132   (Canagaratna et al., 2015), which reflect the relative composition and oxidation degree for

133   different OA source. In our study, PMF was performed on HR mass spectra of OA for ions with

134   m/z values of 12-120, together with the signals from integer m/z values between 121 to 300 (i.e.,

135   unit mass resolution, UMR) using SoFi (version 6.3) in Igor Pro (Paatero, 1999; Canonaco et

136   al., 2013). The data and error matrices were preprocessed according to Elser et al., (2016) and

137   detailed description of PMF analysis was given elsewhere (Canonaco et al. 2013; Elser et al

138   2016). Unconstrained PMF solutions with varied factor numbers were analyzed and six factors

139   were resolved, including two primary and four secondary organic factors (Fig. 3). The six-factor

140   solution was preferred because the five-factor solution was not able to separate high signal of

141   m/z 44 (which represents high oxidation state) from primary organic aerosol (POA) factors,

142   while the seven-factor solution added additional OOA factors with similar profiles and noisy

143   time series for which no physical interpretation could be found. The two POA factors consisted

144   of a traffic-related factor (hydrocarbon-like OA, HOA) and a cooking-related factor (COA),

145   which had been resolved in previous summer studies in NCP (Elser et al., 2016; Hu et al., 2016b;

146   Sun et al., 2016; Huang et al., 2019). AMS source apportionment studies often report one or

147   two oxygenated organic aerosol (OOA) factors that are distinguished by the extent of

148   oxygenation and linked to volatility or oxidation degree. Owing to higher mass resolution of

149   LTOF-AMS and the inclusion of integer-mass signals for m/z from 121 to 300 for high-

150   molecular-weight species such as polycyclic aromatic hydrocarbons (PAHs), we herein

151   resolved four SOA factors. These four SOA factors include aq-SOA attributable to aqueous-

152   phase chemistry, O$_x$-initiated-SOA attributable to photochemistry, primary-related-SOA

153   attributable to prompt oxidation of POA during emission, and fresh-SOA with a lower f_{44}/f_{43}

154   ratio (fraction of m/z 44 and 43 in OA).

2.4 Aerosol liquid water content

The aerosol liquid water content (ALWC) was simulated by ISORROPIA-II model (Fountoukis and Nenes, 2007; Hennigan et al., 2015) using the measurements of ambient inorganic species (NO3, SO4, NH4, and Chl) and meteorological parameters (temperature and RH). The simulation was run in "metastable" mode where all components are assumed to be deliquescent and contain no solid matter. The concentrations and speciation (if dissociated) of those inorganic species in thermodynamic equilibrium was then simulated by the model and then the ALWC was calculated. The inorganic cations such as Na^+, K^+, Ca^{2+}, Mg^{2+} were not measured and included in the simulation on account of that these crustal ions constituted relatively small fractions of aerosol, and had relatively weak effects on ALWC accumulation (Fountoukis and Nenes, 2007;Su et al., 2022). The ISORROPIA-II model does not consider the contribution to ALWC from organics, since inorganic aerosols dominate the water uptake by ambient particles with a contribution of approximate >80% of the total ALWC (Huang et al., 2020).

3. Results and discussion

3.1 SOA sources

In our study, SOA accounted for 69% (13.5 μg m^{-3}) of the total OA (19.6 μg m^{-3}), representing the dominant fraction in OA in summer Handan. Among the four PMF-resolved SOA sources (Fig. 1), O_x-initiated-SOA dominated (31% to total OA), followed by fresh-SOA (18%), aq-SOA (15%), and primary-related-SOA (5%). Since we focus on SOA formation in this study, detailed descriptions of the HOA (12%) and COA (19%) is provided in section 1.1 in the SI. The mass spectral profiles of the six OA source factors are shown in Fig. 1, while the time series of the SOA factors are shown in Fig. 2. In particular, a remarkable continuous growth of aq-SOA concentration (from ~0.3 μg m^{-3} to 25.2 μg m^{-3}) and ALWC (from 3.1 μg m^{-3} to 486.1 μg m^{-3}) occurred on 24th-28th August (Fig. 2d). Meanwhile, the O:C ratio indicative of OA oxidation state displayed a continuous increase from 0.52 to a maximum of 0.93 during this time (Fig. 2e), consistent with the continuous increase in RH (reaching over 95%). This observation hints that during this period aqueous-phase processing might have played an important role in aq-SOA formation. This role of aqueous-phase processing in SOA formation is not just specific to this particular event, but also important in the whole campaign, which is discussed in detail in section 3.3 later.

SOA factors were resolved depending on the oxidation state, which correspond to aged SOA and fresh SOA respectively (Jimenez et al., 2009). One factor is attributed to aqueous-phase chemistry (aq-SOA) and the other to photochemistry (O_x-initiated-SOA), while fresher factor is produced by fresh-source (fresh-SOA) with a lower f_{44}/f_{43} ratio, and the other considered as

189   oxidized primary sources denoted as primary-related-SOA. Although all of the SOA factors
190   were characterized by higher m/z 44 (CO_2^+) and m/z 28 (CO^+) signal compared with POA
191   factors, their mass spectrum and temporal trends were noticeably distinguishable,
192   corresponding to different formation mechanism, which will be discussed in the following
193   section.

194   As shown in Fig. S3, the aq-SOA was identified as it increased with ALWC but decreased
195   with O_x, which might be produced/influenced by aqueous-phase chemistry and is defined as aq-
196   SOA. This indicates that aq-SOA was either formed via aqueous phase reactions or
197   absorbed/dissolved into aerosol liquid water. It exhibits the highest O:C ratios of all factors (0.7)
198   and a higher f_{CO2+} to the total signal of 21.7%, but a low H:C ratio of 1.24 (Fig. 1). The O_x-
199   initiated-SOA in our study is photochemical production SOA whose formation initiated with
200   the presence of O_x. As O_x has been shown to be a conserved tracer to during photochemical
201   processing (Xu et al., 2017), the relationship between O_x and O_x-initiated-SOA can represent a
202   metric to characterize SOA formation mechanisms associated with ozone production chemistry
203   SOA (Herndon et al., 2008). O_x-initiated-SOA presented an opposite trend with significant
204   increase as function of O_x but decreased as a function of ALWC (Fig. S3), suggesting the
205   dominant role of photochemical processing in the formation of O_x-initiated-SOA.

206   The fresh-SOA showed an increase substantially as ALWC increasing, similar to aq-SOA.
207   Whereas it also showed a slight increase trend following O_x when $O_x < 100$ ppb (Fig. S3).
208   Therefore, both aqueous-phase chemistry and photochemical processing were thought to have
209   positive impacts synchronously on the formation of fresh-SOA. In this study, the fresh-SOA
210   had the lowest atomic O:C ratio of 0.41 and the highest atomic H:C ratio of 1.41 among the
211   four SOA factors, corresponding with the f_{CO2+} of 8.3%, these characteristics are consistent with
212   the global average O:C ratio of LO-OOA of 0.35 ± 0.14, Ng et al., 2010), demonstrating the it
213   is more fresh SOA. Although the primary-related-SOA constituted a small fraction and showed
214   little variation during P1~P3 (3%~5%), this SOA source is also of particular interest because
215   of its distinctive fragments with high m/z values in the mass spectrum (Fig. 1d). At $m/z < 120$,
216   the primary-related-SOA had higher intensities for m/z 43 (mainly $C_2H_3O^+$) and m/z 44 (mainly
217   CO_2^+) than those in POA, indicating a typical nature of less-oxidized SOA. At $m/z > 120$, PAH-
218   derived fragments are clearly evident in the mass spectrum of the primary-related-SOA, as
219   indicated by PAH-like ions (described in SI 1.2) (Dzepina et al., 2007). Previous AMS studies
220   have observed pronounced peaks of PAH ions in POA mass spectra, such as those in coal
221   combustion organic aerosol (CCOA) and biomass burning organic aerosol (BBOA) (Hu et al.,
222   2016b; Zhao et al., 2019), but rarely in SOA. This observation implies that the factor may be
223   related to the POA originated from domestic coal combustion and here it is termed as primary-
224   related-SOA (Xu et al., 2006). Moreover, this SOA factor exhibited relatively better
225   correlations with some gaseous pollutants (Fig. S4), such as CO ($R = 0.6$) and NO_2 ($R = 0.5$),

226 and also tracked with HOA ($R = 0.4$). These observations suggest that the primary-related-SOA
227 might be transformed from locally emitted POA as a non-negligible source to SOA.

228 To further investigate the SOA formation mechanism, the dataset was segregated into three
229 periods according to different features depends on meteorological parameters (Fig. 2), i.e., the
230 reference period (P1), high-O_x period (P2) and high-RH period (P3). Briefly, the reference
231 period, P1, was characterized by a low average OA concentration (15.4 ± 3.2 μg m^{-3}) and was
232 mainly affected by clean air from southwest of the sampling site and precipitation activities
233 (Table S1). The high-O_x period (P2) was featured by a high O_x concentration (65.1 ± 20.4 ppb),
234 warmer temperatures (26.4 ± 4.0 ℃) but lower RH (57.7 ± 17.5 %). The mass loadings of OA
235 (19.8 ± 4.7 μg m^{-3}) and other pollutants in P2 were higher than those in P1 (Table S1). P3 was
236 assigned as a high-RH period because of the noticeably high RH (83.7 ± 12.5 %) and high
237 ALWC (95.4 ± 114.2 μg m^{-3}). Winds were weak (<1.0 m s^{-1}) throughout this period, indicative
238 of stagnant conditions, which facilitated pollutant accumulation and resulted in the highest
239 average OA concentrations (25.0 ± 6.2 μg m^{-3}).

240 During the reference period (P1), SOA had the lowest contribution to OA (57%), and the O_x-
241 initiated-SOA and aq-SOA constituted 22% and 21% to total OA, respectively. For the high-
242 O_x period (P2), enhanced SOA formation was found, with the SOA fraction increased to 71%
243 of the total OA. The O_x-initiated-SOA showed the highest mass loading of 7.3 μg m^{-3} and
244 highest contribution of 37% to total OA. These increases suggest that high-O_x condition
245 facilitates the production of SOA by photochemistry, making the O_x-initiated-SOA the major
246 source of SOA during P2. During the high-RH period (P3), SOA fraction continually increased,
247 approaching 79% in total OA, and the SOA was mainly contributed by aq-SOA and fresh-SOA.
248 The mass contribution of aq-SOA increased dramatically from 9% to total OA during P2 to 33%
249 during P3 (Fig. S2), and average mass concentrations from 1.8 μg m^{-3} to 8.3 μg m^{-3}, which
250 suggests rapid SOA production through the aqueous-phase chemistry. Comparatively, the
251 contribution of fresh-SOA was about ~20% in both P2 and P3, but lower in P1 (9%), suggesting
252 that the formation fresh-SOA was affected by both high O_x and high RH. It should also be noted
253 that O:C ratio increased in the succession from P1 (0.73) to P2 (0.74) and further to P3 (0.77),
254 accompanied by continually decrease of H:C ratio from 1.64 to 1.56, and to 1.53 (Fig. 3),
255 suggesting the increase of OA oxidation degree. As a result, the high O_x in P2 and high RH in
256 P3 (as compared to P1) promoted the formation of SOA, specifically O_x-initiated-SOA (in P2)
257 and aq-SOA (in P3), leading to the increase in the degree of oxygenation in total OA.

258 Overall, our results suggest that SOA could be formed through different pathways, in
259 particular photochemistry, aqueous-phase chemistry, and conversion of POA to SOA
260 contributed to SOA formation.

261 **3.2 Photochemistry**

262   As expected for summertime, photochemistry associated with O_x has significant impacts on

263   the formation and evolution of SOA. Herein, the relationships between OA factors and O_x were

264   investigated to offer insights into the formation mechanisms of SOA associated with the ozone

265   production chemistry (Herndon et al., 2008). During P2, as O_x increased, the mass loadings of

266   O_x-initiated-SOA showed a substantially increasing trend when O_x was > 30 ppb and eventually

267   saturated when O_x was >100 ppb, raising the contribution of O_x-initiated-SOA from 20% to 61%

268   of total OA (Fig. 4). This observation indicates the importance of photochemistry in the

269   formation of O_x-initiated-SOA in summer, in which high O_x concentration as well as

270   temperature corresponding to strong atmospheric oxidative capacity, can accelerate the

271   photochemical formation (Duan et al., 2021). As a comparison, the mass concentrations of other

272   OA factors except O_x-initiated-SOA showed decreasing trends as O_x increased (Fig. 4c). Such

273   differences between SOA factors are likely due to the enhanced secondary

274   production/transformation from POA and fresher SOA factors to the more aged O_x-initiated-

275   SOA. Note that the O:C ratio presented a faster increasing rate as a function of O_x (from 0.6 to

276   1.0, Fig. 4d) than those in P1 and P3, suggesting that photochemistry might result in higher OA

277   oxidation state during P2.

278   The typical episode with high-O_x period (P2) was dominated by a series of daytime

279   photochemical evolutions. To evaluate the relative contributions of photochemical and

280   aqueous-phase processing production and the transformation of these SOA factors in different

281   meteorological stages, the average diurnal variations of OA factors, O:C ratios, O_x, temperature,

282   AWLC and primary gas pollutants during different periods are shown for comparison. Fig. 6

283   shows that O_x increased rapidly from 6:00 to 14:00 in all periods, but was highest in

284   P2. Correspondingly, a lower mean value of ALWC (8.4 $\mu g\ m^{-3}$) was also observed in P2 than

285   in P1 and P3. During P2, O_x-initiated-SOA was produced quickly and played the dominant role

286   during daytime, while its concentration typically decreased during nighttime. The average

287   concentration of O_x-initiated-SOA increased continually from 4.2 $\mu g\ m^{-3}$ at 7:00 local time (LT)

288   to 10.4 $\mu g\ m^{-3}$ at 15:00 LT in 8 h, with the maximum O_x-initiated-SOA mass fraction in OA

289   reaching 65% at 15:00 LT (Fig. S6c). This high average growth rate of 0.8 $\mu g\ m^{-3}\ h^{-1}$ in O_x-

290   initiated-SOA corresponded to the high O_x concentration, high temperature and strong solar

291   radiation in daytime, suggesting enhanced photochemistry reaction. In contrast, the

292   concentrations and the contributions of other SOA factors deceased continuously at the same

293   time (Fig. 6). The opposite trends between O_x-initiated-SOA and other OA factors from 7:00

294   to 15:00 LT suggest that some part of POA and fresh-SOA may convert to O_x-initiated-SOA

295   by photochemical oxidation. This conclusion is consistent with findings reported by Li et al.,

296   (2020) in urban Beijing, where less-oxidized SOA may transform to more-oxidized SOA

297   through photochemical processing as well. The O:C ratio of OA presented a significant

298   increasingly diurnal variation with a noon peak around 14:00 ~ 16:00 LT in P2, which had the

299   highest value of 0.74 compared with P1 and P3, suggesting the potential transformation from

300   POA factors and fresh SOA factors to O_x-initiated-SOA could also noticeably affect OA

301   characteristics such as oxidation state in summer daytime. It is further indicated by a small

302   afternoon peak of the more oxidized tracer CO_2^+ (*m/z* 44) and the decrease in a less oxidized

303   tracer $C_2H_3O^+$ (*m/z* 43) (Fig. 7b). As a result, the mass spectra, which were initially fresh SOA

304   products evolved to become aged SOA products as the photochemical age increased. Overall,

305   with little water in the particles, the high solar radiation and high O_x concentration during

306   daytime associated with a relatively high degree of oxygenation of OA suggest that gas-phase

307   oxidation and partitioning processes are probably the dominating process in SOA formation

308   during P2.

309   In addition, these results further support the idea that during the high-O_x period of summer,

310   photochemistry has significant impacts on SOA formation, especially on O_x-initiated-SOA.

311   Note that the role of photochemistry in the formation of O_x-initiated-SOA is not only limited to

312   the gas-phase photochemistry, but also can also occur in the aqueous phase (Kuang et al., 2020).

313   This is the case for P3 in our study, which is discussed further in section 3.3 below.

314   **3.3 Aqueous-phase chemistry**

315   The aqueous-phase chemistry has imposed significant impacts on SOA formation during this

316   field campaign. To further explore the formation mechanism of SOA associated with aqueous-

317   phase chemistry, the relationships between different OA factors and ALWC were investigated.

318   During P3, the mass concentration of aq-SOA increased from 5 μg m^{-3} to 17 μg m^{-3}, yet its

319   fraction showed a particularly pronounced rise from 22.5% to 52% of total OA when ALWC

320   increased from 0.3 to 200 μg m^{-3} (Fig. 5e and f). Note that there are still consistent mass

321   concentrations of aq-SOA even when ALWC is very low (data interval ranging from 0~40 μg

322   m^{-3}), which is due to that over 80% of ALWC mass concentration were loaded in the first

323   interval, leading to a higher mean value of aq-SOA mass concentration. Actually ALWC

324   showed quite low mass loading in most period time but increased dramatically during P3, yet

325   the time series of aq-SOA and ALWC were remarkably well correlated throughout the entire

326   campaign (*R*=0.7, Fig. S4) rather than a strong correlation observed only in P3. This general

327   correlation further confirms the important role of aqueous-phase chemistry in the formation of

328   aq-SOA and characterized the aqueous-phase formation of aq-SOA throughout the campaign

329   rather than only in the high-RH event as shown in section 3.1 earlier. We also found that the

330   concentration and fraction of aq-SOA became stable when ALWC was > 200 μg m^{-3}, which is

331   probably attributable to that the aq-SOA formation within droplets was soon outweighed by the

332   scavenging processes when RH was high enough (> 95%). The O:C ratio shows an obvious

333   increase from 0.7 to around 0.85 when ALWC increases to 200 μg m^{-3}, after which it remains

334 relatively stable (0.85) as the ALWC increases further (Fig. 5). These results suggest that
335 aqueous-phase chemistry can affect the oxidation degree of OA by changing SOA composition,
336 especially the enhanced contribution of aq-SOA. However, the growth rate of O:C ratios as
337 ALWC increases in P3 was lower than that in P2 (up to 1 as O_x increases). Also, the correlation
338 between O:C vs. O_x in P2 (R=0.6) was stronger than O:C vs. ALWC (R=0.3) (Fig. S8).

339   Fig. 6 illustrate the different types of aqueous-phase chemistry in daytime and nighttime.
340 During the nighttime in P3, aqueous-phase oxidation was also enhanced during nighttime
341 (19:00–07:00 LT). As shown in Fig. 6, O:C ratio (0.76) at nighttime in P3 was higher than those
342 in P2, while exhibiting a much smaller peak during daytime. Compared with the low ALWC in
343 P2, the much higher ALWC concentration (peak value of 235.9 μg m^{-3} at 2:00 LT) and higher
344 RH (peak value of 93.7% at 6:00 LT) during nighttime in P3 suggested a dominant contribution
345 by aqueous-phase processing. The aq-SOA shows a quite clear and unique diurnal pattern in
346 P3, with much higher mass concentration during the whole day (especially at nighttime) than
347 those in P1 and P2. After 17:00 LT, aq-SOA started to increase from 4.7 μg m^{-3} to 12.7 μg m^{-3}
348 at 7:00 LT, which showed a rapid nighttime growth rate of 0.6 μg m^{-3} h^{-1}, indicating enhanced
349 SOA formation through aqueous-phase chemistry at night. Whereas O_x-initiated-SOA
350 decreased rapidly from 8.2 μg m^{-3} at 17:00 LT until reaching its lowest concentration of 2.6
351 μg m^{-3} until the morning, suggesting the gas-to-particle partitioning at night under high ALWC
352 conditions. Furthermore, this transformation could be supported by the increase in CO_2^+ (m/z
353 44) and the decrease in a less oxidized tracer $C_2H_3O^+$ (m/z 43) at night (Fig. 7c). Since when
354 the ALWC is sufficiently high, it was likely to accommodate much of the precursor organics
355 and oxidants to low-volatility products through aqueous-phase oxidation. In addition, the dark
356 aqueous-phase SOA formation was likely strong enough to counteract the nighttime scavenging
357 processes under high-RH conditions. Therefore, the dark aqueous-phase chemistry forming aq-
358 SOA shows a dominant role (over 40% to OA) during nighttime in P3.

359   However, during the daytime, the mass concentration of aq-SOA decreased from 7:00 to
360 17:00 LT in P3, coinciding an obvious increase trend of O_x-initiated-SOA at the same time with
361 an average growth rate of 0.6 μg m^{-3} h^{-1} (Fig. 6). This phenomenon suggests photochemical
362 processing can also occur in the aqueous phase when RH and ALWC were still high.
363 Photochemical reactions through both aqueous-phase and gas-phase can contribute
364 substantially to the SOA formation in polluted areas of NCP, and during haze days with high
365 RH and ALWC the aqueous-phase photochemical processes played a dominant role in daytime
366 SOA formation (Kuang et al., 2020). The rapid daytime O_x-initiated-SOA formation in our
367 study possibly occurred on the particle surface and in the aerosol liquid water (Ervens et al.,
368 2011) under humid conditions with high ALWC but driven by gas-phase direct photolysis and
369 oxidation by photooxidants under high O_x conditions. Under such high-RH level (RH > 80%),

370 the water-soluble species produced from photochemistry in the gas phase can also partition into
371 the aqueous phase and be further oxidized to form low-volatility products (Carlton et al., 2007;
372 Sullivan et al., 2016). Previous studies have demonstrated that gas-phase oxidants such as OH
373 radicals and H_2O_2 can also partition to the aqueous phase to further oxidize dissolved the
374 oxidized VOCs (OVOCs) into aq-SOA (Ye et al., 2018). Other studies also revealed that
375 photochemical reactions in the aqueous droplets can occur through direct photolysis or through
376 oxidation by oxidants (Ervens et al., 2011; 2014;Ye et al., 2018). Therefore, in our campaign,
377 dark aqueous-phase chemistry is responsible for rapid aq-SOA formation during nighttime,
378 while the aqueous-phase photochemistry during daytime is likely prevail by rapid daytime O_x-
379 initiated-SOA formation during P3. This comparison demonstrates that the nocturnal aqueous-
380 phase chemistry and daytime aqueous-phase photochemistry are both important pathways in
381 the total SOA growth. The aqueous-phase chemistry related to fresh-SOA is more complicated,
382 requiring both daytime radiative conditions and certain amounts of ALWC in nighttime. For
383 example, Fig. 5e shows that the fresh-SOA has a similar increasing trend with aq-SOA as
384 ALWC increased, however, it also increased slightly as O_x increased (Fig. 4e), hinting that both
385 ALWC and the oxidants are critical for fresh-SOA formation and both the aqueous-phase
386 chemistry and the photochemistry (including that in the aqueous phase) participated to produce
387 fresh-SOA simultaneously. It is worth noting that three peaks were found in the diurnal
388 variation of fresh-SOA in P3. The peaks at around 6:00 and 19:00 LT at night were similar to
389 those of aq-SOA and lower than it, while the peak at around 13:00 LT is consistent with the
390 peak in the diurnal cycle of O_x (Fig. 6). Although there is also a smaller peak around 13:00 LT
391 in P3, the whole pattern of aq-SOA is characterized by decreasing trend at daytime. These
392 results suggest that fresh-SOA could be formed through dark nighttime aqueous-phase reactions,
393 which are partially reversible upon the evaporation of aerosol liquid water, and also formed
394 through photochemical aqueous-phase reactions during daytime. Different from aq-SOA,
395 which is highly correlated and limited with ALWC, two types of aqueous-phase chemistry in
396 daytime and nighttime are dominant pathways to the fresh-SOA growth. Our analysis on
397 formation pathways of these SOA factors suggested the potential interactive roles of gas-phase
398 oxidation, gas-particle partitioning, and aqueous-phase oxidation in the formation of SOA.

399 **3.4 SOA from POA transformation**

400   The photochemistry and aqueous-phase chemistry show distinct effects on POA evolution
401 and SOA formation. The relationships between O_x-initiated-SOA /aq-SOA and other POA-
402 related components (HOA + COA + primary-related-SOA) were plotted in Fig. S9. A strong
403 negative correlation (R=-0.8) between POA-related components and O_x-initiated-SOA was
404 observed (Fig. S9c), consistent with the decrease in mass concentration of POA-related
405 components during P2. This observation suggests that the production of O_x-initiated-SOA was

at least partly facilitated by photochemical transformation of other OA components. However, the better diffusion conditions in P2 might also attribute a great extent to the negative correlation, as the formation period of O_x-initiated-SOA usually occurred during the noontime when the boundary layer was much developed, while the POA usually decreased via horizontal and vertical diffusion. In comparison, POA-related components and aq-SOA correlate weakly. When ALWC (<20 $\mu g\ m^{-3}$) and nitrate concentrations were lower (< 3 $\mu g\ m^{-3}$), mostly during P1 and P2, POA-related components and aq-SOA showed almost no correlation (R=0.1and R=-0.1). However, when ALWC concentration and nitrate concentration were higher than those thresholds above (data points with yellow/red colors mostly during P3), they had a relatively good negative correlation (R=-0.5) (Fig. S9f), indicating the importance of ALWC and nitrate in aqueous-phase chemistry. This is consistent with results in winter Beijing (Wang et al., 2021), where POA factor had strong negative correlations with aq-SOA, suggesting that these POA factors might produce aq-SOA by aqueous-phase oxidation. In addition, under high-ALWC conditions, nitrate had similar formation mechanisms with aq-SOA or high nitrate supports the potential formation/transformation from POA-related components to aq-SOA, which is consistent with the results in section 3.3. The phenomenon of negative correlation between POA-related components and SOA at high O_x/ALWC further emphasizes the importance of conversion from POA to SOA.

As shown in the Van Krevelen (VK) plot (Fig. 8a), O:C and H:C both increase in the succession from primary-related-SOA to O_x-initiated-SOA and eventually to aq-SOA, supporting a successive oxidation sequence from primary-related-SOA to aq-SOA. Generally, H:C shows a decreasing trend as O:C increases for organic compounds during oxidation in other studies (Ng et al., 2011; Gilardoni et al., 2016; Lee et al., 2017: Zhao et al., 2019; Chen et al., 2021), suggesting a general negative correlation between H:C and O:C. This positive relationship of O:C and H:C evolution during oxidative aging in this study is interesting. It might be caused by ring-breaking reactions which could further promote the transformation of aromatic POA to aq-SOA. Previous studies in both laboratory (Huang et al., 2018; Wang et al., 2020) and field (Hu et al., 2016a) demonstrated that the OH-initiated ring-breaking reactions of aromatic species can occur in the aqueous phase and form highly oxidized oxygenated compounds. For example, Hems and Abbatt (2018) suggested that nitrophenol molecules could react rapidly with OH radicals in aqueous solutions with the addition of OH functional groups to the aromatic ring at the initial stage, followed by fragmentation to multifunctional organic species with high H:C and O:C ratios. Wang et al. (2021) found that the ring-breaking oxidation of aromatic FF-POA was the mechanism for aq-SOA formation. Similar to those in primary-related-SOA, PAH-like ions was also found in the mass spectrum of aq-SOA at $m/z > 150$, albeit less pronounced, consistent with a previous study in Beijing (Wang et al., 2021). This is likely due to the oxidation of PAHs in the conversion of primary-related-SOA and aq-SOA,

443   which is caused by enhanced hydroxylation of the aromatic ring and increased yields of

444   carboxylic acids in OH-initiated reactions (Sun et al., 2010). This kind of ring-breaking

445   oxidation of aromatic POA could thus lead to aq-SOA formation (Huang et al., 2018; Wang et

446   al., 2021). In addition, the locations of aq-SOA and the slope of overall OA are near the line

447   with the slope of -1 in the VK plot, indicating more carboxylic acid formation while the

448   replacement of a hydrogen atom with a carboxylic acid group (−COOH) (Heald et al., 2010;

449   Ng et al., 2011). This observation supports that oxidation of PAHs was probably involved in

450   the conversion of primary-related-SOA to aq-SOA through aqueous-phase chemistry, leading

451   to functionalization as carbonyls and carboxylic acids.

452   Specifically, the organic fragments and mass spectrum evolution of OA were analyzed to

453   illuminate the transformation in photochemical processing and aqueous-phase chemistry. Fig.

454   8b shows the mass fractions of $CH_2O_2^+$, CH_3SO^+, HCO_2^+, and $C_2H_2O_2^+$ ion fragments in OA as

455   a function of ALWC. The aq-SOA was tightly correlated with $CH_2O_2^+$ ($R^2 = 0.81$) at m/z 46

456   and CH_3SO ($R^2 = 0.78$) at m/z 63 (Fig. S10), Consistently, both of them showed increase trends

457   as ALWC increasing, similar as aq-SOA, which indicating typical fragment characteristics of

458   ions of aqueous-phase processing products (Tan et al., 2009; Sun et al., 2016; Duan et al., 2021).

459   The intensities of HCO_2^+ (m/z 45), a common fragment ion of carboxylic acids, is associated

460   with aqueous oxidation of aromatic compounds. $C_2H_2O_2^+$ (m/z 58) is a tracer ion for glyoxal,

461   which could be a ring-breaking product from the aqueous-phase oxidation of PAHs. The

462   increasing trends of these ions with ALWC suggest that water-soluble organic species such as

463   carboxylic acids and glyoxal are produced as components of aq-SOA following aromatic

464   oxidation and ring breaking. Moreover, the concentration of PAHs increased with the increase

465   of ALWC (Fig. S11), consistent with the oxidation of PAHs from ring-breaking reactions that

466   can take place in the aqueous phase and being involved in the conversion to aq-SOA.

467   **4. Conclusion**

468   The sources and formation mechanisms of SOA were investigated by online aerosol mass

469   spectrometry and statistical (PMF) analysis from August to September of 2019 in Handan, a

470   mid-sized industrialized city in NCP of China. Four specific SOA factors were resolved,

471   including aq-SOA (15% to total OA), O_x-initiated-SOA (31%), fresh-SOA (18%) and primary-

472   related-SOA (5%). By studying the formation of these SOA factors in different selected periods

473   (P1-P3) against O_x and ALWC, we found multiple pathways leading to their formation,

474   sometimes with mixed pathways for one type of SOA.

475   Both photochemistry and aqueous-phase chemistry resulted in enhanced OA oxidation state.

476   During high-O_x period, photochemistry had imposed significant impacts on the formation and

477   evolution of SOA in summertime. The O_x-initiated-SOA contributed up to 65% to total OA in

the daytime, with a high average growth rate of $0.8\,\mu g\,m^{-3}\,h^{-1}$, suggesting the efficient daytime formation of SOA from photochemistry. Rapid increases of the concentration and contribution (up to 61%) of O_x-initiated-SOA were found as O_x increased, while all the other OA factors showed decreasing trends with O_x concentration increasing. The difference suggests enhanced secondary transformation from POA/fresh SOA factors to the more aged O_x-initiated-SOA under high-O_x condition. However, during the high-RH period, two types of aqueous-phase chemistry were both important pathways for the SOA growth. During nighttime and under high-RH conditions, dark aqueous-phase chemistry played significant roles with rapid aq-SOA formation (up to 45% in total OA), while the aqueous-phase photochemistry was more important by rapid O_x-initiated-SOA formation during daytime (up to 39% in total OA). The primary-related-SOA was evidently linked to the POA originated from coal combustion activities, as indicated by the PAH-like ion peaks. Although it constituted a small fraction of 5%, the potential transformation and conversion from primary-related-SOA to aq-SOA could also be an important pathway via hydroxylation of the aromatic ring or ring-breaking oxidation of aromatic POA species through aqueous-phase chemistry. This study highlights the multiple reaction pathways, on top of multiple precursor types, on the SOA formation in industrialized regions, and calls form more in-depth study on the interactive roles of those formation pathways.

Data availability. Raw data used in this study are archived at the Institute of Earth Environment, Chinese Academy of Sciences, and are available on request by contacting the corresponding author.

Supplement. The Supplement related to this article is available online.

Competing interests. The authors declare that they have no conflict of interest.

Author contributions. RJH designed the study. Data analysis and source apportionment were done by YFG and RJH. YFG and RJH wrote the manuscript. YFG and RJH interpreted data and prepared display items. All authors commented on and discussed the manuscript.

Acknowledgement

This work was supported by the National Natural Science Foundation of China (no. 41925015), the Key Research Program of Frontier Sciences from the Chinese Academy of Sciences (no. ZDBS-LY-DQC001), the Strategic Priority Research Program of the Chinese Academy of Sciences (no. XDB40000000), and SKLLQG (no. SKLLQGTD1801).

References

An, Z., Huang, R. J., Zhang, R., Tie, X., Li, G., Cao, J., Zhou, W., Shi, Z., Han, Y., Gu, Z., and Ji, Y.: Severe haze in northern China: A synergy of anthropogenic emissions and atmospheric processes, Proc. Natl. Acad. Sci. U. S. A., 116, 8657–8666, https://doi.org/10.1073/pnas.1900125116, 2019.

Bikkina, S., Kawamura, K., and Sarin, M.: Secondary Organic Aerosol Formation over Coastal Ocean: Inferences from Atmospheric Water-Soluble Low Molecular Weight Organic Compounds, Environ. Sci. Technol., 51, 4347–4357, https://doi.org/10.1021/acs.est.6b05986, 2017.

Canagaratna, M. R., Jimenez, J. L., Kroll, J. H., Chen, Q., Kessler, S. H., Massoli, P., Hildebrandt Ruiz, L., Fortner, E., Williams, L. R., Wilson, K. R., Surratt, J. D., Donahue, N. M., Jayne, J. T., and Worsnop, D. R.: Elemental ratio measurements of organic compounds using aerosol mass spectrometry: Characterization, improved calibration, and implications, Atmos. Chem. Phys., 15, 253–272, https://doi.org/10.5194/acp-15-253-2015, 2015.

Canonaco, F., Crippa, M., Slowik, J. G., Baltensperger, U., and Prévôt, A. S. H.: SoFi, an IGOR-based interface for the efficient use of the generalized multilinear engine (ME-2) for the source apportionment: ME-2 application to aerosol mass spectrometer data, Atmos. Meas. Tech., 6, 3649–3661, https://doi.org/10.5194/amt-6-3649-2013, 2013.

Carlton, A. G., Turpin, B. J., Altieri, K. E., Seitzinger, S., Reff, A., Lim, H. J., and Ervens, B.: Atmospheric oxalic acid and SOA production from glyoxal: Results of aqueous photooxidation experiments, Atmos. Environ., 41, 7588–7602, https://doi.org/10.1016/j.atmosenv.2007.05.035, 2007.

Chen, W., Ye, Y., Hu, W., Zhou, H., Pan, T., Wang, Y., Song, W., Song, Q., Ye, C., Wang, C., Wang, B., Huang, S., Yuan, B., Zhu, M., Lian, X., Zhang, G., Bi, X., Jiang, F., Liu, J., Canonaco, F., Prevot, A. S. H., Shao, M., and Wang, X.: Real-time characterization of aerosol compositions, sources and aging processes in Guangzhou during PRIDE-GBA 2018 campaign, J. Geophys. Res. Atmos., https://doi.org/10.1029/2021jd035114, 2021.

Cohen, A. J., Brauer, M., Burnett, R., Anderson, H. R., Frostad, J., Estep, K., Balakrishnan, K., Brunekreef, B., Dandona, L., Dandona, R., Feigin, V., Freedman, G., Hubbell, B., Jobling, A., Kan, H., Knibbs, L., Liu, Y., Martin, R., Morawska, L., Pope, C. A., Shin, H., Straif, K., Shaddick, G., Thomas, M., van Dingenen, R., van Donkelaar, A., Vos, T., Murray, C. J. L., and Forouzanfar, M. H.: Estimates and 25-year trends of the global burden of disease attributable to ambient air pollution: an analysis of data from the Global Burden of Diseases Study 2015, Lancet, 389, https://doi.org/10.1016/S0140-6736(17)30505-6, 2017.

Donahue, N. M., Robinson, A. L., Stanier, C. O., and Pandis, S. N.: Coupled partitioning, dilution, and chemical aging of semivolatile organics, Environ. Sci. Technol., 40, https://doi.org/10.1021/es052297c, 2006.

Duan, J., Huang, R. J., Gu, Y., Lin, C., Zhong, H., Wang, Y., Yuan, W., Ni, H., Yang, L., Chen, Y., Worsnop, D. R., and O'Dowd, C.: The formation and evolution of secondary organic aerosol during summer in Xi'an: Aqueous phase processing in fog-rain days, Sci. Total Environ., 756, 144077, https://doi.org/10.1016/j.scitotenv.2020.144077, 2021.

Dzepina, K., Arey, J., Marr, L. C., Worsnop, D. R., Salcedo, D., Zhang, Q., Onasch, T. B., Molina, L. T., Molina, M. J., and Jimenez, J. L.: Detection of particle-phase polycyclic aromatic hydrocarbons in Mexico City using an aerosol mass spectrometer, Int. J. Mass Spectrom., 263, 152–170, https://doi.org/10.1016/j.ijms.2007.01.010, 2007.

Elser, M., Huang, R., Wolf, R., Slowik, J. G., Wang, Q., Canonaco, F., Li, G., Bozzetti, C., Daellenbach, K. R., Huang, Y., Zhang, R., Li, Z., Cao, J., Baltensperger, U., El-haddad, I., and Prévôt, A. S. H.: New insights into PM 2 . 5 chemical composition and sources in two major cities in China during extreme haze events using aerosol mass spectrometry, 3207–3225, https://doi.org/10.5194/acp-16-3207-2016, 2016.

Ervens, B., Turpin, B. J., and Weber, R. J.: Secondary organic aerosol formation in cloud droplets and aqueous particles (aqSOA): A review of laboratory, field and model studies, Atmos. Chem. Phys., 11, 11069–11102, https://doi.org/10.5194/acp-11-11069-2011, 2011.

Ervens, B., Armin, S., B., L. Y., and J., and T. B.: Key parameters controlling OH-initiated formation of secondary organic aerosol in the aqueous phase (aqSOA), J. Geophys. Res., 6578–6595, https://doi.org/10.1002/2013JD021021.Received, 2014.

Fountoukis, C. and Nenes, A.: ISORROPIAII: A computationally efficient thermodynamic equilibrium model for K+-Ca2+-Mg2+-NH4+-Na+-SO42--NO3--Cl--H2O aerosols, Atmos. Chem. Phys., 7, 4639–4659, https://doi.org/10.5194/acp-7-4639-2007, 2007.

Gilardoni, S., Massoli, P., Paglione, M., Giulianelli, L., Carbone, C., Rinaldi, M., Decesari, S., Sandrini, S., Costabile, F., and Gobbi, G. P.: Direct observation of aqueous secondary organic aerosol from biomass-burning emissions, Proc. Natl. Acad. Sci. U. S. A., 113, 10013–10018, https://doi.org/10.1073/pnas.1602212113, 2016.

Gu, Y., Huang, R. J., Li, Y., Duan, J., Chen, Q., Hu, W., Zheng, Y., Lin, C., Ni, H., Dai, W., Cao, J., Liu, Q., Chen, Y., Chen, C., Ovadnevaite, J., Ceburnis, D., and O'Dowd, C.: Chemical nature and sources of fine particles in urban Beijing: Seasonality and formation mechanisms, Environ. Int., 140, 105732, https://doi.org/10.1016/j.envint.2020.105732, 2020.

Heald, C. L., Kroll, J. H., Jimenez, J. L., Docherty, K. S., Decarlo, P. F., Aiken, A. C., Chen, Q., Martin, S. T., Farmer, D. K., and Artaxo, P.: A simplified description of the evolution of organic aerosol composition in the atmosphere, Geophys. Res. Lett., 37, https://doi.org/10.1029/2010GL042737, 2010.

Hems, R. F. and Abbatt, J. P. D.: Aqueous Phase Photo-oxidation of Brown Carbon Nitrophenols: Reaction Kinetics, Mechanism, and Evolution of Light Absorption, ACS Earth Sp. Chem., 2, 225–234, https://doi.org/10.1021/acsearthspacechem.7b00123, 2018.

Hennigan, C. J., Izumi, J., Sullivan, A. P., Weber, R. J., and Nenes, A.: A critical evaluation of proxy methods used to estimate the acidity of atmospheric particles, Atmos. Chem. Phys., 15, 2775–2790, https://doi.org/10.5194/acp-15-2775-2015, 2015.

Herndon, S. C., Onasch, T. B., Wood, E. C., Kroll, J. H., Canagaratna, M. R., Jayne, J. T., Zavala, M. A., Knighton, W. B., Mazzoleni, C., Dubey, M. K., Ulbrich, I. M., Jimenez, J. L., Seila, R., de Gouw, J. A., de Foy, B., Fast, J., Molina, L. T., Kolb, C. E., and Worsnop, D. R.: Correlation of secondary organic aerosol with odd oxygen in Mexico City, Geophys. Res. Lett., 35, https://doi.org/10.1029/2008GL034058, 2008.

Hu, W., Hu, M., Hu, W. W., Niu, H., Zheng, J., Wu, Y., Chen, W., Chen, C., Li, L., Shao, M., Xie, S., and Zhang, Y.: Characterization of submicron aerosols influenced by biomass burning at a site in the Sichuan Basin, southwestern China, Atmos. Chem. Phys., 16, 13213–13230, https://doi.org/10.5194/acp-16-13213-2016, 2016a.

Hu, W., Hu, M., Hu, W., Jimenez, J. L., Yuan, B., Chen, W., Wang, M., Wu, Y., Chen, C., Wang, Z., Peng, J., Zeng, L., and Shao, M.: Journal of Geophysical Research : Atmospheres, 1955–1977, https://doi.org/10.1002/2015JD024020.Received, 2016b.

Hu, W., Palm, B. B., Day, D. A., Campuzano-Jost, P., Krechmer, J. E., Peng, Z., De Sa Suzane, S., Martin, S. T., Alexander, M. L., Baumann, K., Hacker, L., Kiendler-Scharr, A., Koss, A. R., De Gouw, J. A., Goldstein, A. H., Seco, R., Sjostedt, S. J., Park, J. H., Guenther, A. B., Kim, S., Canonaco, F., Prévôt, A. S. H., Brune, W. H., and Jimenez, J. L.: Volatility and lifetime against OH heterogeneous reaction of ambient isoprene-epoxydiols-derived secondary organic aerosol (IEPOX-SOA), Atmos. Chem. Phys., 16, 11563–11580, https://doi.org/10.5194/acp-16-11563-2016, 2016c.

Hu, W., Hu, M., Hu, W., Zheng, J., Chen, C., Wu, Y., and Guo, S.: Seasonal variations in high time-resolved chemical compositions , sources , and evolution of atmospheric submicron aerosols in the megacity Beijing, 9979–10000, 2017.

Huang, D. D., Zhang, Q., Cheung, H. H. Y., Yu, L., Zhou, S., Anastasio, C., Smith, J. D., and Chan, C. K.: Formation and Evolution of aqSOA from Aqueous-Phase Reactions of Phenolic Carbonyls: Comparison between Ammonium Sulfate and Ammonium Nitrate Solutions, Environ. Sci. Technol., 52, 9215–9224, https://doi.org/10.1021/acs.est.8b03441, 2018.

Huang, R. J., Zhang, Y., Bozzetti, C., Ho, K. F., Cao, J. J., Han, Y., Daellenbach, K. R., Slowik, J. G., Platt, S. M., Canonaco, F., Zotter, P., Wolf, R., Pieber, S. M., Bruns, E. A., Crippa, M., Ciarelli, G., Piazzalunga, A., Schwikowski, M., Abbaszade, G., Schnelle-Kreis, J., Zimmermann, R., An, Z., Szidat, S., Baltensperger, U., El Haddad, I., and Prévôt, A. S. H.: High secondary aerosol contribution to particulate pollution during haze events in China, Nature, 514, 218–222, https://doi.org/10.1038/nature13774, 2014.

Huang, R. J., Wang, Y., Cao, J., Lin, C., Duan, J., Chen, Q., Li, Y., Gu, Y., Yan, J., Xu, W., Fröhlich, R., Canonaco, F., Bozzetti, C., Ovadnevaite, J., Ceburnis, D., Canagaratna, M. R., Jayne, J., Worsnop, D. R., El-Haddad, I., Prevot, A. S. H., and O'Dowd, C. D.: Primary

624   emissions versus secondary formation of fine particulate matter in the most polluted city
625   (Shijiazhuang) in North China, Atmos. Chem. Phys., 19, 2283–2298,
626   https://doi.org/10.5194/acp-19-2283-2019, 2019.

627 Huang, R. J., He, Y., Duan, J., Li, Y., Chen, Q., Zheng, Y., Chen, Y., Hu, W., Lin, C., Ni, H.,
628   Dai, W., Cao, J., Wu, Y., Zhang, R., Xu, W., Ovadnevaite, J., Ceburnis, D., Hoffmann, T.,
629   and D. ODowd, C.: Contrasting sources and processes of particulate species in haze days
630   with low and high relative humidity in wintertime Beijing, Atmos. Chem. Phys., 20, 9101–
631   9114, https://doi.org/10.5194/acp-20-9101-2020, 2020.

632 Jimenez, J. L., Jayne, J. T., Shi, Q., Kolb, C. E., Worsnop, D. R., Yourshaw, I., Seinfeld, J. H.,
633   Flagan, R. C., Zhang, X., Smith, K. A., Morris, J. W., and Davidovits, P.: Ambient aerosol
634   sampling using the Aerodyne aerosol mass spectrometer, J. Geophys. Res. Atmos., 108, 1–
635   13, https://doi.org/10.1029/2001jd001213, 2003.

636 Jimenez, J. L., Canagaratna, M. R., Donahue, N. M., Prevot, A. S. H., Zhang, Q., Kroll, J. H.,
637   DeCarlo, P. F., Allan, J. D., Coe, H., Ng, N. L., Aiken, A. C., Docherty, K. S., Ulbrich, I.
638   M., Grieshop, A. P., Robinson, A. L., Duplissy, J., Smith, J. D., Wilson, K. R., Lanz, V. A.,
639   Hueglin, C., Sun, Y. L., Tian, J., Laaksonen, A., Raatikainen, T., Rautiainen, J., Vaattovaara,
640   P., Ehn, M., Kulmala, M., Tomlinson, J. M., Collins, D. R., Cubison, M. J., Dunlea, E. J.,
641   Huffman, J. A., Onasch, T. B., Alfarra, M. R., Williams, P. I., Bower, K., Kondo, Y.,
642   Schneider, J., Drewnick, F., Borrmann, S., Weimer, S., Demerjian, K., Salcedo, D., Cottrell,
643   L., Griffin, R., Takami, A., Miyoshi, T., Hatakeyama, S., Shimono, A., Sun, J. Y., Zhang,
644   Y. M., Dzepina, K., Kimmel, J. R., Sueper, D., Jayne, J. T., Herndon, S. C., Trimborn, A.
645   M., Williams, L. R., Wood, E. C., Middlebrook, A. M., Kolb, C. E., Baltensperger, U., and
646   Worsnop, D. R.: Evolution of organic aerosols in the atmosphere, Science (80-.)., 326,
647   1525–1529, https://doi.org/10.1126/science.1180353, 2009.

648 Kuang, Y., He, Y., Xu, W., Yuan, B., Zhang, G., Ma, Z., Wu, C., Wang, C., Wang, S., Zhang,
649   S., Tao, J., Ma, N., Su, H., Cheng, Y., Shao, M., and Sun, Y.: Photochemical Aqueous-Phase
650   Reactions Induce Rapid Daytime Formation of Oxygenated Organic Aerosol on the North
651   China Plain, Environ. Sci. Technol., 54, 3849–3860,
652   https://doi.org/10.1021/acs.est.9b06836, 2020.

653 Lee, A. K. Y., Chen, C. L., Liu, J., Price, D. J., Betha, R., Russell, L. M., Zhang, X., and Cappa,
654   C. D.: Formation of secondary organic aerosol coating on black carbon particles near
655   vehicular emissions, Atmos. Chem. Phys., 17, 15055–15067, https://doi.org/10.5194/acp-
656   17-15055-2017, 2017.

657 Li, H., Zhang, Q., Zhang, Q., Chen, C., Wang, L., Wei, Z., Zhou, S., Parworth, C., Zheng, B.,
658   Canonaco, F., Prévôt, A. S. H., Chen, P., Zhang, H., Wallington, T. J., and He, K.:
659   Wintertime aerosol chemistry and haze evolution in an extremely polluted city of the North
660   China Plain: Significant contribution from coal and biomass combustion, Atmos. Chem.
661   Phys., 17, 4751–4768, https://doi.org/10.5194/acp-17-4751-2017, 2017.

Li, J., Liu, Z., Gao, W., Tang, G., Hu, B., Ma, Z., and Wang, Y.: Insight into the formation and evolution of secondary organic aerosol in the megacity of Beijing, China, Atmos. Environ., 220, https://doi.org/10.1016/j.atmosenv.2019.117070, 2020.

Middlebrook, A. M., Bahreini, R., Jimenez, J. L., and Canagaratna, M. R.: Evaluation of composition-dependent collection efficiencies for the Aerodyne aerosol mass spectrometer using field data, Aerosol Sci. Technol., 46, 258–271, https://doi.org/10.1080/02786826.2011.620041, 2012.

Ng, N. L., Canagaratna, M. R., Zhang, Q., Jimenez, J. L., Tian, J., Ulbrich, I. M., Kroll, J. H., Docherty, K. S., Chhabra, P. S., Bahreini, R., Murphy, S. M., Seinfeld, J. H., Hildebrandt, L., Donahue, N. M., Decarlo, P. F., Lanz, V. A., Prévôt, A. S. H., Dinar, E., Rudich, Y., and Worsnop, D. R.: Organic aerosol components observed in Northern Hemispheric datasets from Aerosol Mass Spectrometry, Atmos. Chem. Phys., 10, 4625–4641, https://doi.org/10.5194/acp-10-4625-2010, 2010.

Ng, N. L., Canagaratna, M. R., Jimenez, J. L., Chhabra, P. S., Seinfeld, J. H., and Worsnop, D. R.: Changes in organic aerosol composition with aging inferred from aerosol mass spectra, Atmos. Chem. Phys., 11, 6465–6474, https://doi.org/10.5194/acp-11-6465-2011, 2011.

Onasch, T. B., Trimborn, A., Fortner, E. C., Jayne, J. T., Kok, G. L., Williams, L. R., Davidovits, P., and Worsnop, D. R.: Soot particle aerosol mass spectrometer: Development, validation, and initial application, Aerosol Sci. Technol., 46, 804–817, https://doi.org/10.1080/02786826.2012.663948, 2012.

Paatero, P.: The Multilinear Engine—A Table-Driven, Least Squares Program for Solving Multilinear Problems, Including the n-Way Parallel Factor Analysis Model, J. Comput. Graph. Stat., 8, 854–888, https://doi.org/10.1080/10618600.1999.10474853, 1999.

Sullivan, A. P., Hodas, N., Turpin, B. J., Skog, K., Keutsch, F. N., Gilardoni, S., Paglione, M., Rinaldi, M., Decesari, S., Cristina Facchini, M., Poulain, L., Herrmann, H., Wiedensohler, A., Nemitz, E., Twigg, M., and Collett, J. L.: Evidence for ambient dark aqueous SOA formation in the Po Valley, Italy, Atmos. Chem. Phys., 16, 8095–8108, https://doi.org/10.5194/acp-16-8095-2016, 2016.

Su, J., Zhao, P., Ge, S., and Ding, J.: Aerosol liquid water content of PM2.5 and its influencing factors in Beijing, China, Sci. Total Environ., 839, 156342, https://doi.org/10.1016/j.scitotenv.2022.156342, 2022.

Sun, Y., Chen, C., Zhang, Y., Xu, W., Zhou, L., Cheng, X., Zheng, H., Ji, D., Li, J., Tang, X., Fu, P., and Wang, Z.: Rapid formation and evolution of an extreme haze episode in Northern China during winter 2015, 1–9, https://doi.org/10.1038/srep27151, 2016.

Sun, Y., Xu, W., Zhang, Q., Jiang, Q., Canonaco, F., Prévôt, A. S. H., Fu, P., Li, J., Jayne, J., Worsnop, D. R., and Wang, Z.: Source apportionment of organic aerosol from 2-year highly time-resolved measurements by an aerosol chemical speciation monitor in Beijing, China, Atmos. Chem. Phys., 18, 8469–8489, https://doi.org/10.5194/acp-18-8469-2018, 2018a.

Sun, Y., Xu, W., Zhang, Q., Jiang, Q., Canonaco, F., and Prévôt, A. S. H.: Source apportionment of organic aerosol from two-year highly time- resolved measurements by an aerosol chemical speciation monitor in Beijing , China, 2018b.

Sun, Y. L., Zhang, Q., Anastasio, C., and Sun, J.: Insights into secondary organic aerosol formed via aqueous-phase reactions of phenolic compounds based on high resolution mass spectrometry, Atmos. Chem. Phys., 10, 4809–4822, https://doi.org/10.5194/acp-10-4809-2010, 2010.

Wang, J., Ye, J., Zhang, Q., Zhao, J., Wu, Y., Li, J., Liu, D., Li, W., Zhang, Y., Wu, C., Xie, C., Qin, Y., Lei, Y., Huang, X., Guo, J., Liu, P., Fu, P., Li, Y., Lee, H. C., Choi, H., Zhang, J., Liao, H., Chen, M., Sun, Y., Ge, X., Martin, S. T., and Jacob, D. J.: Aqueous production of secondary organic aerosol from fossil-fuel emissions in winter Beijing haze, Proc. Natl. Acad. Sci. U. S. A., 118, 1–6, https://doi.org/10.1073/pnas.2022179118, 2021.

Wang, S., Newland, M. J., Deng, W., Rickard, A. R., Hamilton, J. F., Muñoz, A., Ródenas, M., Vázquez, M. M., Wang, L., and Wang, X.: Aromatic Photo-oxidation, A New Source of Atmospheric Acidity, Environ. Sci. Technol., 54, 7798–7806, https://doi.org/10.1021/acs.est.0c00526, 2020.

Xu, S., Liu, W., and Tao,   and S.: Emission of Polycyclic Aromatic Hydrocarbons in China, Biophys. Process. Anthropog. Org. Compd. Environ. Syst., 40, 267–281, https://doi.org/10.1002/9780470944479.ch11, 2006.

Xu, W., Han, T., Du, W., Wang, Q., Chen, C., Zhao, J., Li, J., Fu, P., Wang, Z., Worsnop, D. R., and Sun, Y.: Effects of Aqueous-phase and Photochemical Processing on Secondary Organic Aerosol Formation and Evolution in Beijing , China, https://doi.org/10.1021/acs.est.6b04498, 2017.

Xu, W., Sun, Y., Wang, Q., Zhao, J., Wang, J., Ge, X., Xie, C., Zhou, W., Du, W., Li, J., Fu, P., Wang, Z., Worsnop, D. R., and Coe, H.: Changes in Aerosol Chemistry From 2014 to 2016 in Winter in Beijing: Insights From High-Resolution Aerosol Mass Spectrometry, J. Geophys. Res. Atmos., 124, 1132–1147, https://doi.org/10.1029/2018JD029245, 2019.

Ye, C., Liu, P., Ma, Z., Xue, C., Zhang, C., Zhang, Y., Liu, J., Liu, C., Sun, X., and Mu, Y.: High H2O2 Concentrations Observed during Haze Periods during the Winter in Beijing: Importance of H2O2 Oxidation in Sulfate Formation, Environ. Sci. Technol. Lett., 5, 757–763, https://doi.org/10.1021/acs.estlett.8b00579, 2018.

Zhang, Q., Jimenez, J. L., Canagaratna, M. R., Ulbrich, I. M., Ng, N. L., Worsnop, D. R., and Sun, Y.: Understanding atmospheric organic aerosols via factor analysis of aerosol mass spectrometry: A review, https://doi.org/10.1007/s00216-011-5355-y, 2011.

Zhao, J., Qiu, Y., Zhou, W., Xu, W., Wang, J., Zhang, Y., Li, L., Xie, C., Wang, Q., Du, W., Worsnop, D. R., Canagaratna, M. R., Zhou, L., Ge, X., Fu, P., Li, J., Wang, Z., Donahue, N. M., and Sun, Y.: Organic Aerosol Processing During Winter Severe Haze Episodes in Beijing, J. Geophys. Res. Atmos., 124, 10248–10263, https://doi.org/10.1029/2019JD030832, 2019.

739

740 **Figures**
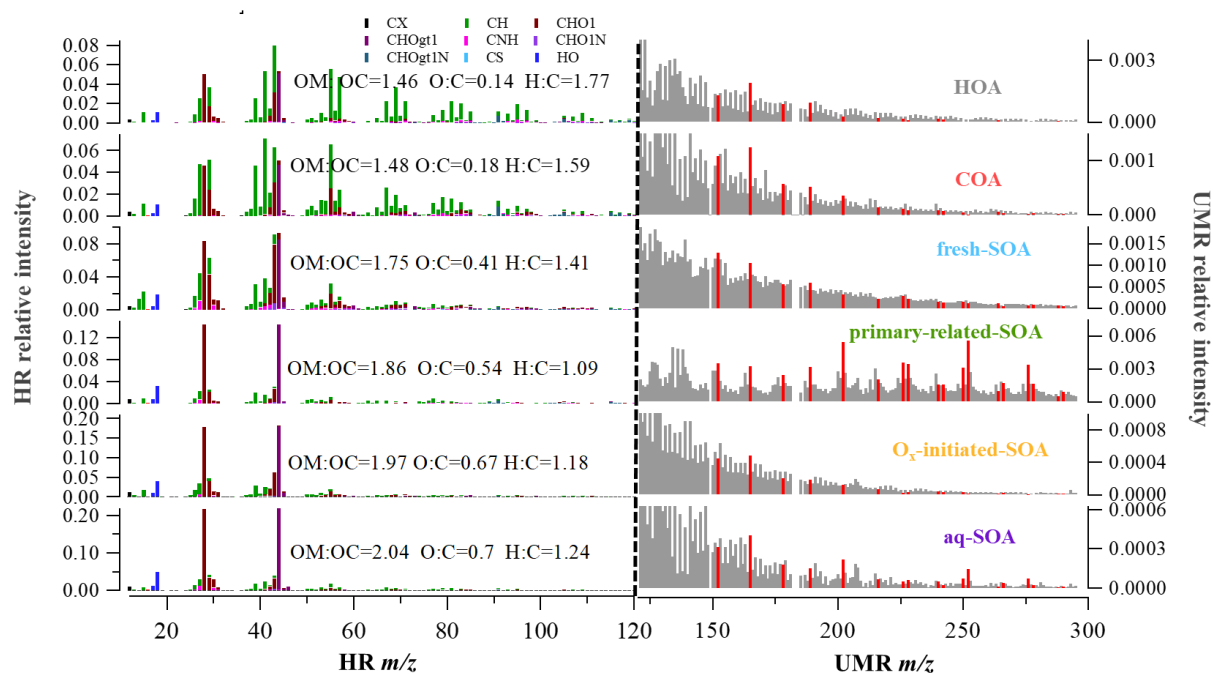
741

742 **Fig. 1** HR and UMR mass spectra of OA factors: (a) HOA; (b) COA; (c) fresh-SOA; (d)
743 primary-related-SOA; (e) O_x-initiated-SOA; (f) aq-SOA. Mass spectra signals less than 120
744 amu are colored by nine ion categories, signals equal to or greater than 120 amu are in unit
745 mass resolution, and polycyclic aromatic hydrocarbons (PAHs) signals are in red on the right
746 panels.

747

748

749
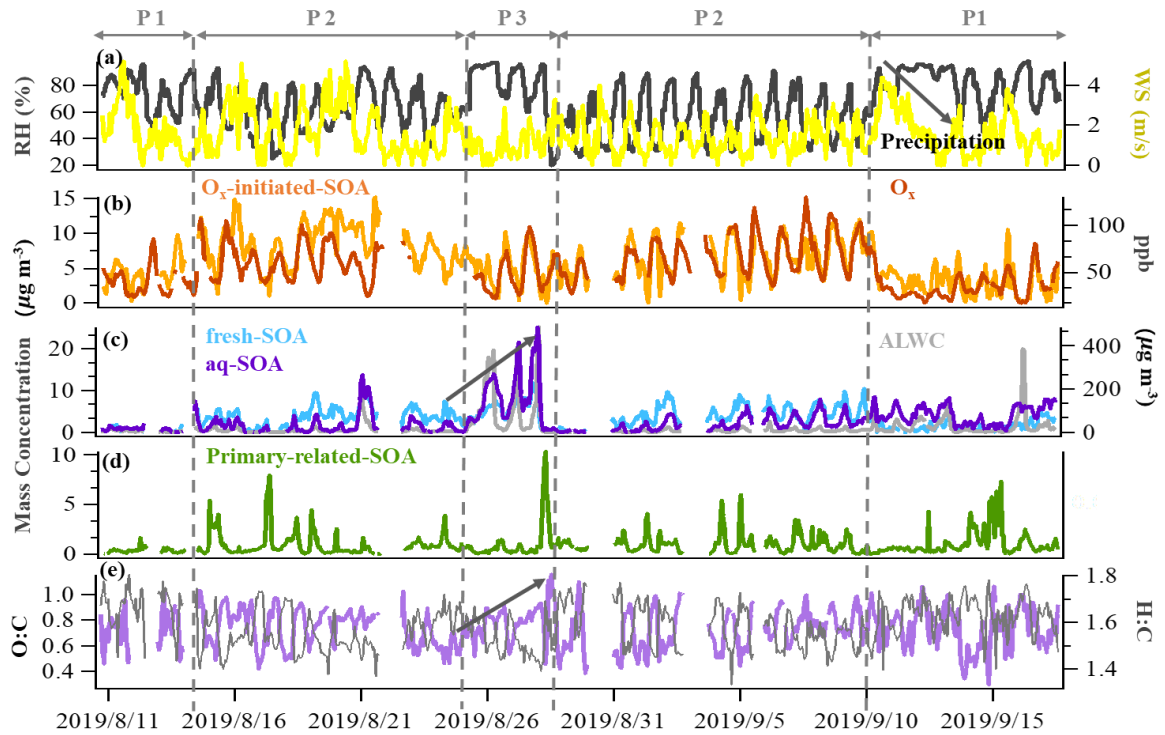
Fig. 2 Time series of (a) relative humidity (RH) and wind speed (WS), (b) O_x and O_x-initiated-SOA, (c) fresh-SOA, aq-SOA and ALWC, (d) primary-related-SOA, (e) the O:C ratio and H:C ratio. The time series were categorized to be three typical periods based on total SOA mass concentrations and meteorology conditions: reference period (P1), high O_x period (P2) and high RH period (P3).

755

756
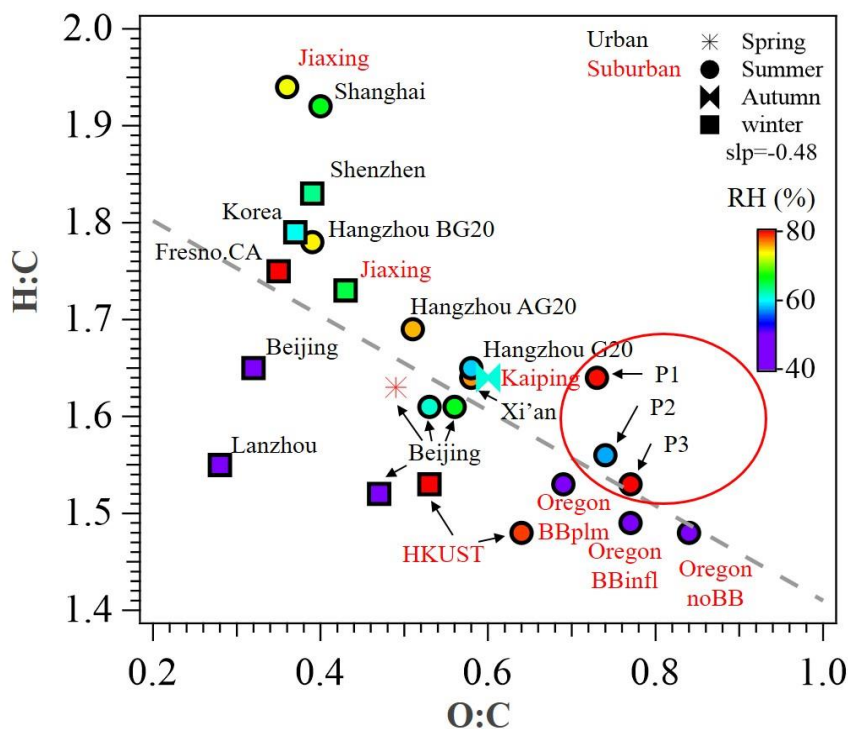
Fig.3 Van Krevelen plot for OA of urban and suburban sites in China and other nations. Data points are colored by RH (%). P1, P2 and P3 in red circles represents the different periods in this study. All the data and related references can be found in Table S3.

760
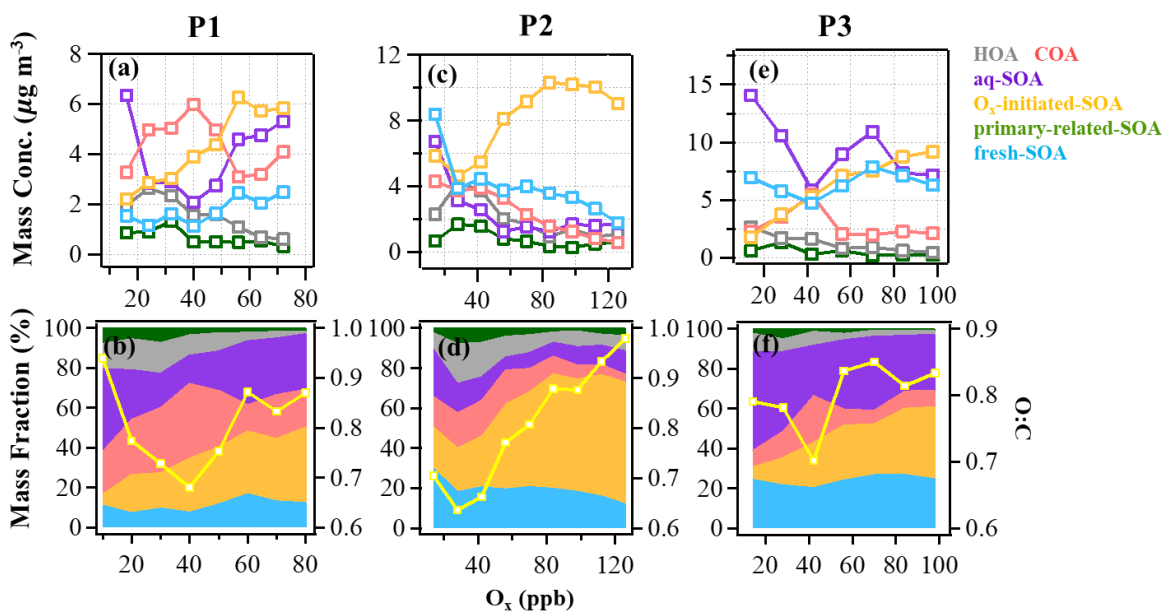
Fig. 4 The mass concentration and contribution of OA factors as functions of O_x in reference period (P1: a & b), high O_x period (P2: c & d) and high RH period (P3: e & f) during this

763   campaign. The yellow curves represent the O:C ration vs. O$_x$. The data were binned according

764   to O$_x$ concentration (10 ppb increment in P1, 14 ppb increment in P2 and P3.

765
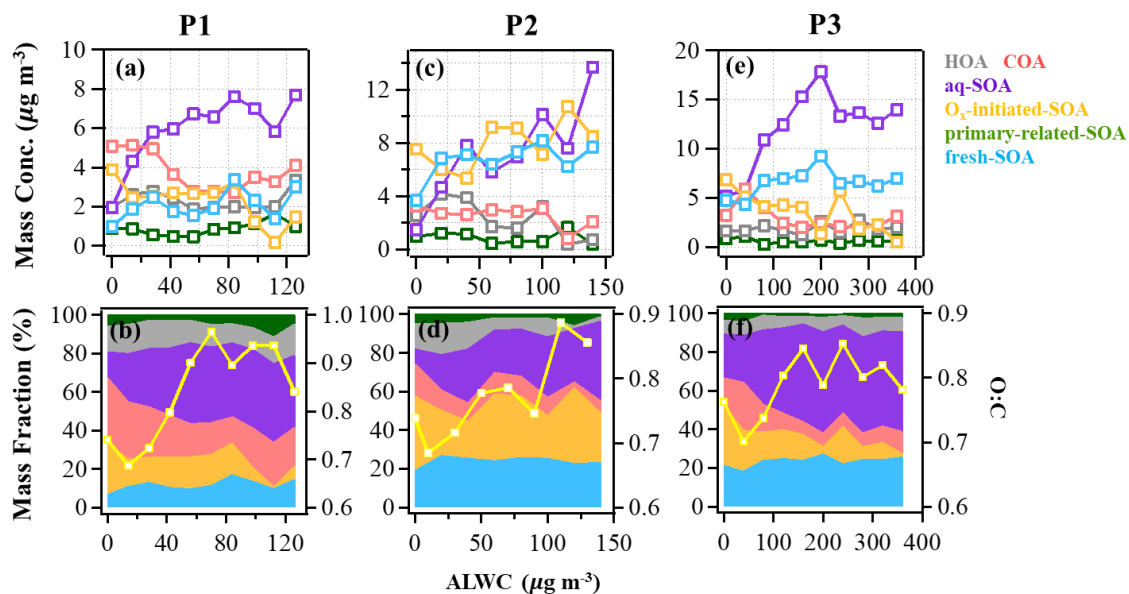
Fig. 5 The mass concentration and contribution of OA factors as functions of ALWC in reference period (P1: a & b), high O$_x$ period (P2: c & d) and high RH period (P3: e & f) during this campaign. The yellow curves represent the O:C ration v.s. ALWC. The data were binned according to the ALWC concentration (14 μgm^{-3}, 20 μgm^{-3} and 40 μgm^{-3} increment in P1 P2 and in P3).
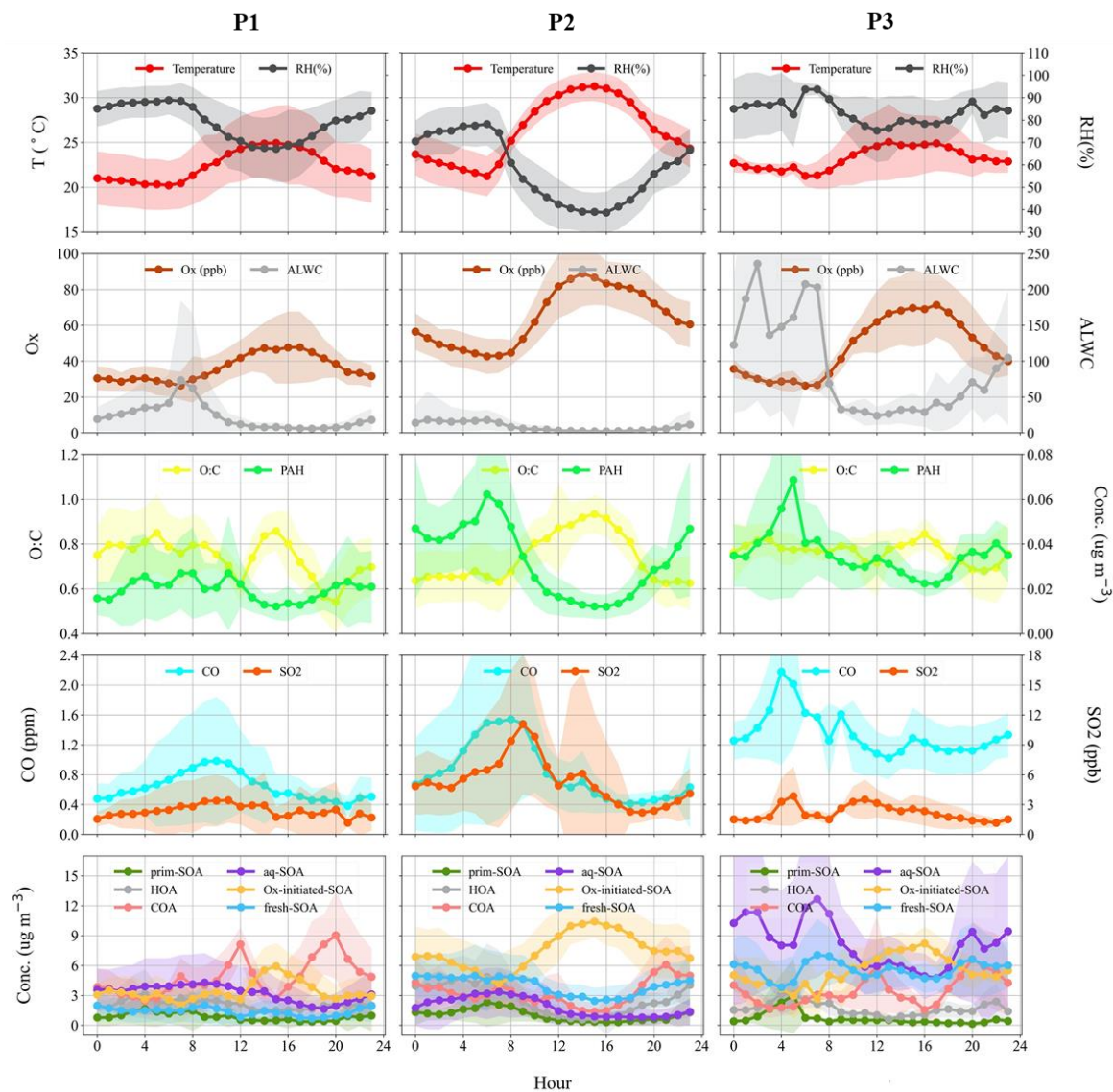
771

772 **Fig. 6** Diurnal patterns of meteorological parameters (T, RH), gaseous species (O_x, CO, SO_2),
773 ALWC (liquid water content), O:C (oxygen-to-carbon elemental ratio), polycyclic aromatic
774 hydrocarbons (PAHs) fragments and OA factors in reference period (P1), high O_x period (P2)
775 and high RH period (P3) in this campaign.
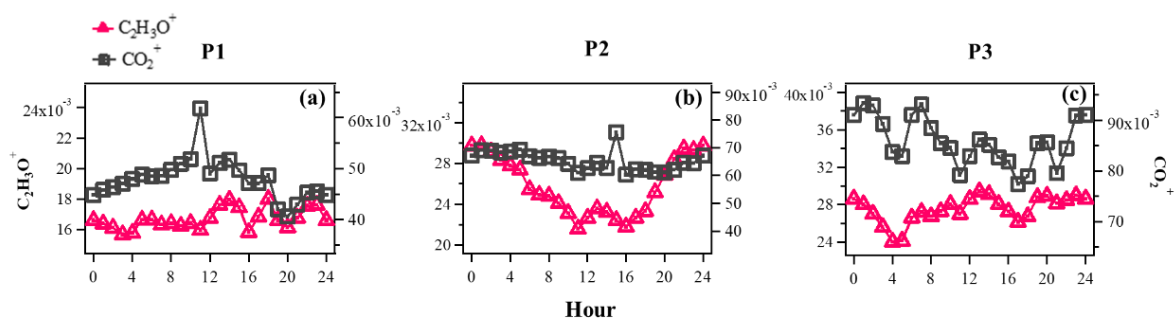
776

777 **Fig. 7** Evolution of high-resolution organic mass spectra on changes in relative intensities (mass
778 fraction) of oxygen-containing ions: $C_2H_3O^+$ (*m/z* 43) and CO_2^+ (*m/z* 44) in reference period
779 (P1:a), high O_x period (P2: b) and high RH period (P3: c) in this campaign.

780
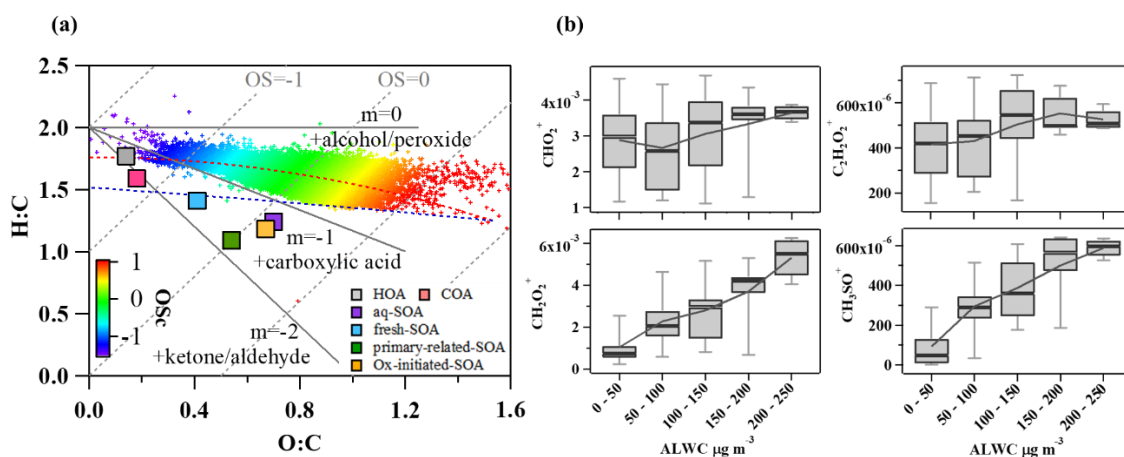
781

782 **Fig. 8** (a) Van Krevelen diagram for the O:C and H:C ratios of different OA factors (marked
783 with squares) and bulk of OA during summer (marked with plus signs and colored by
784 Osccarbon oxidation state (OSc)); (b) Mass fractions of ion fragments indicative of aqueous-
785 phase processing and oxygenated functional groups (alcohols, carboxylic acids) as a function
786 of ALWC.